DSO Velocity Inversion: A "Gas Cloud" Synthetic Example

William W. Symes

August, 1992

TR92-23

Report Documentation Page

Form Approved
OMB No. 0704-0188

1. REPORT DATE	2. REPORT TYPE	3. DATES COVERED
AUG 1992		**00-00-1992 to 00-00-1992**

4. TITLE AND SUBTITLE	5a. CONTRACT NUMBER
DSO Velocity Inversion: A 'Gas Cloud' Synthetic Example	5b. GRANT NUMBER
	5c. PROGRAM ELEMENT NUMBER
6. AUTHOR(S)	5d. PROJECT NUMBER
	5e. TASK NUMBER
	5f. WORK UNIT NUMBER
7. PERFORMING ORGANIZATION NAME(S) AND ADDRESS(ES) **Computational and Applied Mathematics Department ,Rice University,6100 Main Street MS 134,Houston,TX,77005-1892**	8. PERFORMING ORGANIZATION REPORT NUMBER
9. SPONSORING/MONITORING AGENCY NAME(S) AND ADDRESS(ES)	10. SPONSOR/MONITOR'S ACRONYM(S)
	11. SPONSOR/MONITOR'S REPORT NUMBER(S)

12. DISTRIBUTION/AVAILABILITY STATEMENT
Approved for public release; distribution unlimited

13. SUPPLEMENTARY NOTES

14. ABSTRACT

15. SUBJECT TERMS

16. SECURITY CLASSIFICATION OF:			17. LIMITATION OF ABSTRACT	18. NUMBER OF PAGES	19a. NAME OF RESPONSIBLE PERSON
a. REPORT	b. ABSTRACT	c. THIS PAGE			
unclassified	**unclassified**	**unclassified**		**26**	

DSO Velocity Inversion: a "Gas Cloud" Synthetic Example

William W. Symes

The Rice Inversion Project
Department of Computational and Applied Mathematics
Rice Unversity
Houston, Texas 77005

March 2, 1993

Abstract

A low velocity near surface anomaly delays the seismic wavefield and focuses wavefronts passing through it. Such anomalies occur as a result of localized gas seepages ("gas clouds") in the sedimentary column, for example. Use of a migration velocity model not containing the anomaly will produce images containing false synclinal structures. Application of DSO velocity inversion to a simple example of this type images the velocity anomaly and removes the false structure.

Acknowlegement: This work was partially supported by the National Science Foundation (DMS8905878), the Office of Naval Research (N00014-89-J-1115), the Defense Advanced Research Projects Agency and the Air Force Office of Scientific Research (AFOSR 90-0334), the Texas Geophysical Parallel Computation Project, and The Rice Inversion Project. TRIP Sponsors for 1992 are Amoco Research, Conoco Inc., Cray Research, Earth Modeling Systems, Exxon Production Research Co., and Mobil Research and Development Corp.

Introduction

Localized anomalies in otherwise mildly structured subsurface velocity fields pose an interesting challenge to velocity estimation from reflection data. Identification of anomalies is both simpler than the estimation of general laterally heterogeneous structures and more complex than inversion of layered models. Anomalies may be fast, modeling permafrost or salt intrusions, or slow, modeling localized gas-bearing rocks. An example of a slow anomaly caused by the presence of gas sands and its effect on reflection field data appears in Biondi's recent work [1]. Biondi uses a semblance measure based on beam stacks to estimate the heterogeneity and correctly image the structure under the sands.

This paper treats a simple synthetic example in which an otherwise layered velocity field is altered by inclusion of a circular low-velocity zone. The physics of wave propagation used in our experiments is 2D constant density primaries-only acoustics, which is the simplest theory within which the questions asked here may be posed. The reflectivity structure of this model is flat. However prestack migration (or linearized inversion) of data "shot" over this model, using a layered velocity model not containing the anomaly, produces synclines and more complicated non-flat features. The object of our excercise is: working only with the waveform data, estimate the velocity sufficiently accurately to image the correct, flat underlying reflector structure.

For this purpose we use *differential semblance optimization* ("DSO"), a variant of least-squares inversion. DSO has been described at length elsewhere; here we include only a very brief synopsis of the method. The DSO approach combines elements of migration velocity analysis, traveltime tomography and nonlinear inversion. In particular, DSO works directly with waveform data, yet produces velocity estimates closely resembling the output of traveltime inversion. DSO is based on a variational principle. Optimum estimates are approximated by a special iterative minimization algorithm.

For the example constructed here, DSO succeeded in removing almost all of the false structure in two iterations. The velocity anomaly is also imaged. The reconstructed velocity shows the hallmarks of tomographic inversion: smearing along the source/receiver raypaths, oscillation in the orthogonal direction. This is so even though no times are picked, no rays are traced and

no raypath backprojections are performed (explicitly). Only combinations of simulations and migrations are used in the DSO process. Nonetheless DSO produced a kinematically correct velocity, of much the same quality as is obtained by a functional traveltime inversion. In this case at least, DSO performed "tomography without picking".

Velocity inversion *via* DSO

This section gives a brief overview of the 2D primaries only constant density acoustic model and differential semblance optimization in that context. For a more complete account see [6], [7], and [3].

The principal components of the acoustic model discussed here are

- $p(x,z,t)$ = pressure field
- $p_0(x,z,t)$ = reference pressure field
- $v(x,z)$ = velocity field (smooth)
- $r(x,z)$ = reflectivity field ($\sim 2\delta v/v$) (rough)

In addition we regard as known:

- $f(t)$ = source time function (oscillatory)
- $x_s \in$ {source locations}
- $x_r \in$ {receiver locations}
- $t \in$ {time interval}

The source time function $f(t)$ could be included amongst the unknowns as well, at the cost of added computational expense.

These quantities are connected by the coupled wave equations

$$\left(\frac{1}{v(x)^2}\frac{\partial^2}{\partial t^2} - \nabla_x^2\right) p_0(x_s,x,t) = f(t)\delta(x - x_s)$$

$$\left(\frac{1}{v(x)^2}\frac{\partial^2}{\partial t^2} - \nabla_x^2\right) p(x_s,x,t) = r(x)\nabla^2 p_0(x_s,x,t)$$

plus appropriate initial and boundary conditions. The first equation is the usual acoustic wave equation for radiation from an isotropic point source. The second is the perturbational equation for pressure fluctuations $p(x,z,t)$ due to the velocity perturbation $r = \delta v/v$, i.e. the primary reflection or singly scattered field.

Reflection data is predicted by the *forward map*:

$$F[v,r] = \{p(x_s, x_r, t)\}$$

For simplicity receiver arrays are simplified to points $\{x_r\}$ as well.

The reflection data inversion problem may be stated:

$$\begin{gathered}\text{given: } F_{data} = \{p_{data}(x_s, x_r, t)\} \\ \text{find: velocity } v\text{; reflectivity } r \\ \text{so that}\end{gathered}$$

$$F[v,r] \simeq F_{data}$$

As have many others, we formulate this task as a *best-fit problem, via* the *least squares principle* (see e.g. [9]):

$$\text{choose } v, r \text{ to minimize}$$

$$\|F[v,r] - F_{data}\|^2$$

$$(\|...\| = L^2 \text{ norm} = \text{mean square fit error})$$

The nature of this variational problem follows from key properties of the forward map $F[v,r] = \{p(x_s, x_r, t)\}$, which is

- linear in r
- very nonlinear in v

Consequently the mean square fit error $\|F[v,r] - F_{data}\|^2$ is

- quadratic in r, but

- highly nonquadratic (nonconvex) in v

Critical consequences for the least squares principle are:

- estimation of r (oscillatory) given v (smooth) is relatively easy: there are many algorithms, and all work relatively well;
- estimation of v and r simultaneously is very difficult;
- least-squares inversion for v appears to requires nonconvex (global) optimization (Monte-Carlo, simulated annealing...).

Many other velocity indicators, for example the widely used NMO-based velocity spectrum [8] and Biondi's beam stack semblance [1], share the highly nonquadratic nature of the least squares principle for velocities. These are not the only variational principles one can imagine for determination of v and r however. For reasons discussed extensively in the references, we have pursued a different variational principle, *differential semblance optimization*, or DSO. Its key properties are:

- it is a modification of the least-squares principle, and can in fact be regarded as an *infeasible point method* for finding the least squares solution;
- it regards the model for each experiment (x_s) as independent:

$$r = r(x_s, x) \ \text{(but } v = v(x)\text{)}$$

- since in fact the model should not be x_s-dependent (infeasible - "there is only one earth!"), a penalty for infeasibility is added to the mean square fit error to produce the augmented objective function

$$\frac{1}{2}\{|F[v,r] - F_{data}|^2 + \sigma^2|\partial r/\partial x_s|^2\}$$

- Minimization of this objective is accomplished in two stages: minimize first over r (in which the objective is quadratic!) to produce a function of v:

$$J_\sigma[v] = minimum_{r(x_s,x)}\frac{1}{2}\{|F[v,r] - F_{data}|^2 + \sigma^2|\partial r/\partial x_s|^2\}$$

then minimize J_σ over v.

- Note that computing J_σ requires solution of "inner" inverse problem for r given v.

The first term of the differential semblance objective forces the model to fit each shot gather *independently.* The second term measures the *semblance* of neighboring reflectivity inversions in a differential sense; in practice a divided difference is used in place of the derivative with respect to x_s. Since *neighboring* reflectivity gathers are compared, reflectivity gathers are similar even when v is substantially wrong. Thus the differential semblance measure changes much more smoothly than do global measures such as stack power. *Inverted* reflectivities are compared, rather than migrated images with uncontrolled amplitudes. Therefore simple differences are sufficiently robust to measure semblance. This could not be the case if migrated images were used instead, as in migration velocity analysis.

Analysis of and numerical experiments with DSO show that

- J_σ is smooth and convex over a large domain in model space for small σ^2
- if data noise is small, the global minimizer of DSO is close to the global solution of least-squares problem
- The DSO Hessian is closely related to the Hessian of the travel time tomography objective function (this observation is due to Hua Song).

Our implementation includes special devices to ensure accurate calculation of the gradient of J_σ. This calculation is the basis of a nonlinear conjugate gradient algorithm using the Polak-Ribiere step update formula ([2]) for minimizing the DSO objective function. More discussion and a detailed description of the implementation of DSO used here is found in [3].

The Model

The velocity model used in our experiments was based on a layered background v_{strat}, profiled in Figure 1, with velocities ranging from 1.5 m/ms near the surface to 1.9 m/ms at 1200 m depth. This background model was depressed by roughly 12% in a circular region of diameter 400 m centered 500 m below the surface, to produce the target velocity model v_{exact} field shown in Figure 2. The reflectivity field r_{exact} used with v_{exact} to generate the data is horizontally stratified, with profile shown in Figure 3.

A small reflection survey of 30 shots over this model was simulated using a finite difference method of fourth order accuracy in space and second order accuracy in time. The shot spacing was 100 m and shot depth was 8 m. The first shot was located roughly 1400 m to the west (left) of the anomaly center, the last an equal distance to the east (right). The source was punctual, as described in the last section. Thirty four point receivers spaced 50 m apart at 12 m were distributed between 150 m and 1800 m offset to the east (right) of the shot points. Sample intervals in space for the simulation were 16 m in both directions. The sample interval in time was 4 ms. The record length was 2000 ms. The source, regarded as known in these experiments, was a Ricker wavelet of peak frequency 15 Hz.

Selected shot gathers are displayed in Figure 4. The moveout distortion due to the velocity anomaly is clearly visible and moves across the gather as the shot position varies from west to east over the anomaly. A stack of the 30 shot-dependent reflectivities obtained by inversion at the layered background velocity v_{strat} of Figure 1 is displayed as Figure 5. This stack may be viewed as a prestack migration image, and is very similar kinematically to the prestack least squares inversion diplayed in Figure 6. Both images show the expected pull-down below the anomaly, which has become a sinusoidal undulation at the strong reflector at 1300 m due to the formation of a caustic. A similar effect in the migration of a field data set may be observed in Figures 4, 6, and 7 of [1].

DSO inversion

Several parameter choices are required by DSO at this stage in its development. It seems likely that many of these choices could be made automatically, but at present all are made by trial and error. Two of the most important of these paramters are the differential semblance weight σ and the length scale of the allowed velocity models. After some experimentation we chose $\sigma = 0.01$. The length scale (i.e. degree of smoothness) of the velocity model is controlled by choice of norm in velocity space, rather than by parsimonious parameterization (e.g. [1]) to avoid bias. The norm/smoothing mechanism is described in [3]. We chose norm parameters to suppress wavelengths in the velocity shorter than roughly 400 m in these experiments.

Figure 7 displays some common depth point gathers (or common reflection point gathers or coherency panels) for the reflectivity estimate at v_{strat}. Considerable moveout is visible; just as in migration velocity analysis, this indicates a need to update the velocity model (see e.g. [10] for many examples of this idea).

The gradient of the reduced DSO objective function at the layered background velocity:

$$gradJ_\sigma[v_{strat}]$$

is shown in Figure 8. The vertical smearing and side lobes are characteristic of limited aperture tomography; compare for example [5], upper left part of Figure 6 which has similar geometry. Nontheless the location and extent of the anomaly is already well defined. Note that no *a priori* information about either the location or size of the anomaly has been provided.

Two steps of the nonlinear conjugate gradient algorithm produced the velocity model v_2 displayed in Figure 9. The low velocity zone is correctly identified, modulo the vertical smearing noted earlier. The reflectivity CDP gathers for this model (Figure 10) show that most of the residual moveout has been removed. Moreover the stacked reflectivities (Figure 11) are much flatter; the maximum deflection in the center of the synclinal structures has decreased from about 50 m in Figure 6 or 7 to less than 10 m in Figure 9, which is close to optimal given the bandwidth of the data. It seems likely that further iterations could remove at least some of the very mild remaining

structure, which is now roughly 10% of a wavelength in vertical extent.

Conclusion

This synthetic example, while extremely simple, shows that DSO is capable of resolving lateral velocity heterogeneities. As we have shown elsehwere ([3]) that DSO effectively estimates layered structures beginning with quite inaccurate starting models, we might hope that DSO will provide kinematically correct estimates of rather arbitrarily heterogeneous velocity fields.

A major drawback of the current implementation is its computational expense: the two iterations used here required roughly 140 simulations and migrations of the entire data set, and cost about 10 Cray Y-MP CPU hours. This cost, and even the projected cost of more accurate inversions with higher frequency content and larger models, is far smaller than the projected cost of stochastic least squares inversion as proposed for instance by [4]. Nonetheless it is larger than one would like, and will hamper experimentation for some time to come unless reduced.

In the experiments reported here, more than 95% of the CPU cycles were spent in finite difference simulation and migration, which runs at about 250 Mflops on the Y-MP. This is roughly 70% of the peak floating point throughput of the Y-MP CPU; somewhat higher Mflops ratings are achieved with larger models, though the total CPU time goes up considerably. Therefore the speed of the finite difference portion of the code is essentially hardware-limited, and we must look elsewhere for significant software-driven speedup. We are experimenting with improvements in the optimization algorithm, preconditioning of the inner (reflectivity) inversion, and parallelization over shots on both distributed and shared memory architectures, amongst other devices all aimed at a considerably faster implementation.

References

[1] B. BIONDI. Velocity Estimation by Beam Stack, *Geophysics*, 57:1034–1047, 1992.

[2] R. FLETCHER. *Practical methods of optimization, I:Unconstrained Optimization.* Wiley & Sons, New York, 1980.

[3] M. KERN and W. W. SYMES. Inversion of reflection seismograms by differential semblance analysis: algorithm structure and synthetic examples Technical Report 92-3, Department of Computational and Applied Mathematics, Rice University, Houston Texas 77005 USA, 1992.

[4] J.A. SCALES, M. L. SMITH, and T. L. FISCHER. Global optimization methods for highly nonlinear inverse problems. In G. Cohen, L. Halpern, and P. Joly, editors, *Mathematical and Numerical Aspects of Wave Propagation Phenomena*, pages 434–444. SIAM, Philadelphia, 1991.

[5] C. STORK and R. CLAYTON. Using constraints to address the uncertainties of automated prestack velocity analysis. *Geophysics*, 57:404–419, 1992.

[6] W. W. SYMES. The reflection inverse problem for acoustic waves In G. Cohen, L. Halpern, and P. Joly, editors, *Mathematical and Numerical Aspects of Wave Propagation Phenomena*, pages 424–433. SIAM, Philadelphia, 1991.

[7] W. W. SYMES. A differential semblance criterion for inversion of multioffset seismic reflection data. *J. Geophys. Res.*, 1992. to appear.

[8] M. T. TANER and F. KOEHLER. Velocity spectra: digital computer derivation and application of velocity functions. *Geophysics*, 34:859–881, 1969.

[9] A. TARANTOLA. *Inverse Problem Theory.* Elsevier, 1987.

[10] R. VERSTEEG and G. GRAU. Practical aspects of inversion: The Marmousi experience. Proceedings of the EAEG, The Hague, 1991.

Figure Captions

1. Profile of stratified background velocity model v_{strat}.

2. Velocity model v_{exact} used to generate data. Near-surface velocity is 1.5 m/ms; lowest velocity in upper part of anomaly is roughly 1.4 m/ms. High velocity below 1100 m is 1.9 m/ms. Horizontal tick marks are trace number; traces are spaced 16 m apart.

3. Profile of stratified reflectivity model r_{exact}.

4. Selected shot gathers. Vertical scale is ms; trace offset interval is 50 m, far offset is 1800 m. A mute has been applied to remove direct and refracted energy.

5. Stack of inverted reflectivities at the stratified velocity model of Figure 1. Scales are same as Figure 2. Note distinct pulldown, becoming sinusoidal below a coustic at the bottom of the display.

6. Result of least squares inversion (also performed with the DSO software - it does both!). Compare Figure 5.

7. CDP gathers of reflectivity inverted at stratified model, from 1000 m west to 1000 m east of the anomaly. CDP separation is 200 m. Note the considerable moveout over the center section, which is affected by the anomaly. This is a clear indication of velocity error.

8. Gradient of the DSO objective function J_σ at the stratifiec background velocity v_{strat} (Figure 1). Comparing with Figure 2, see that anomaly is already located rather precisely. Typical tomographic raypath smearing and side lobes are present. Scales same as Figure 2.

9. Velocity estimate after 2 nonlinear conjugate gradient steps. Compare Figure 2.

10. CDP gathers of reflectivity inverted at model of Figure 9. Compare Figure 7; note that gathers are essentially flat.

11. Stacked reflectivities inverted at model of Figure 9. Compare Figures 5 and 6; note that false structure is almost entirely removed.

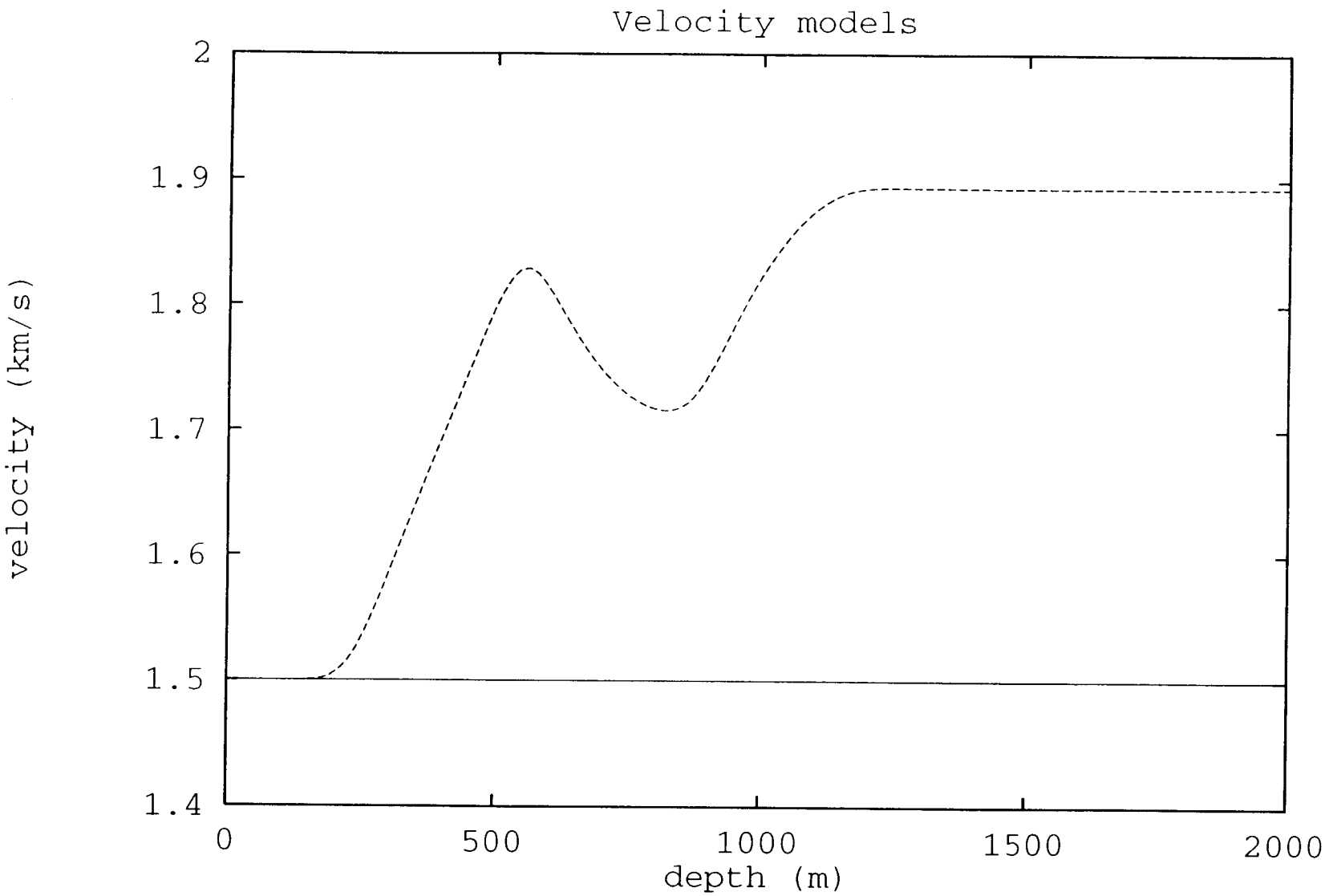
Velocity models
velocity (km/s)
2
1.9
1.8
1.7
1.6
1.5
1.4
0
500
1000
1500
2000
depth (m)

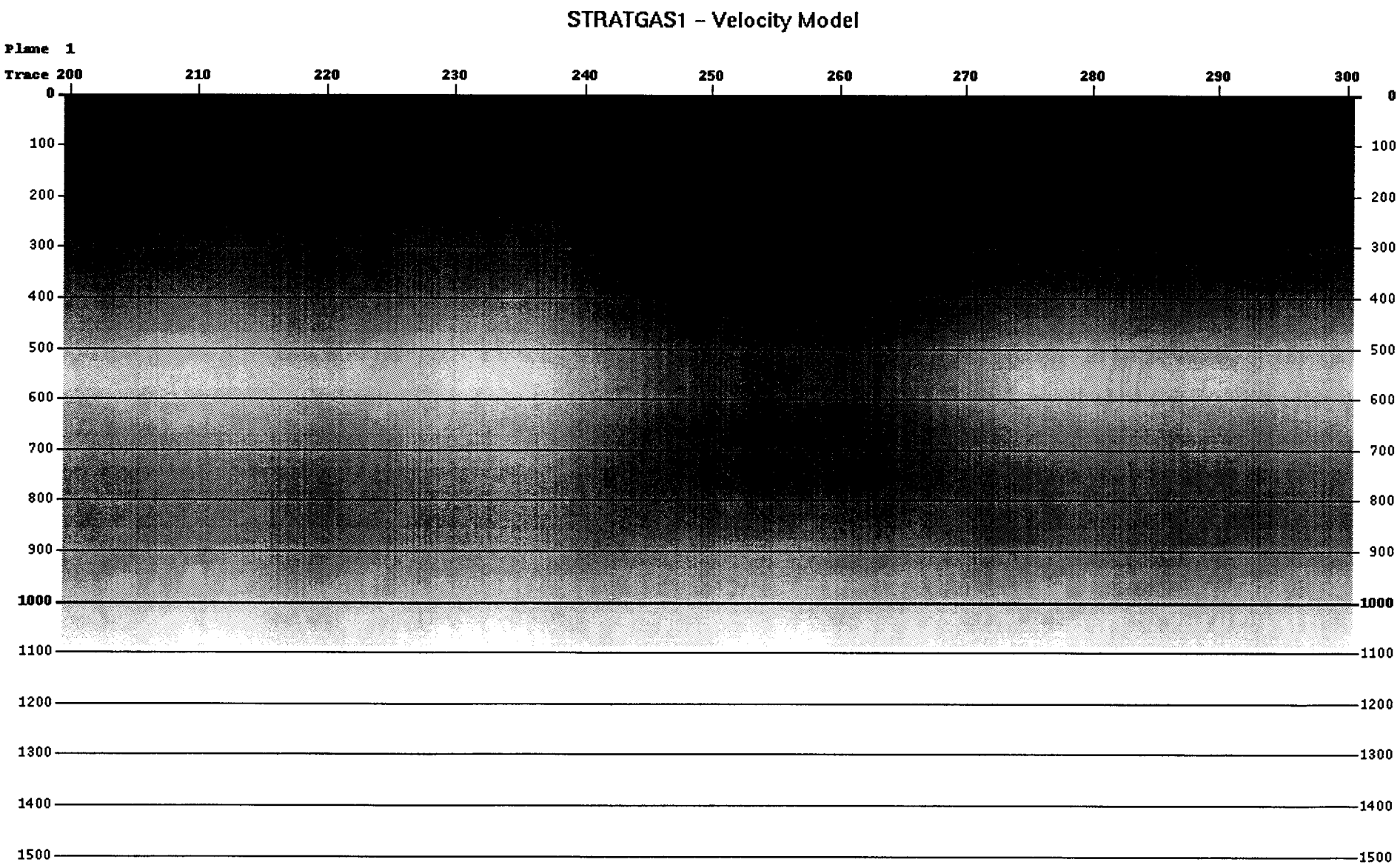
STRATGAS1 – Velocity Model
Plane 1
Trace 200
210
220
230
240
250
260
270
280
290
300
0
100
200
300
400
500
600
700
800
900
1000
1100
1200
1300
1400
1500

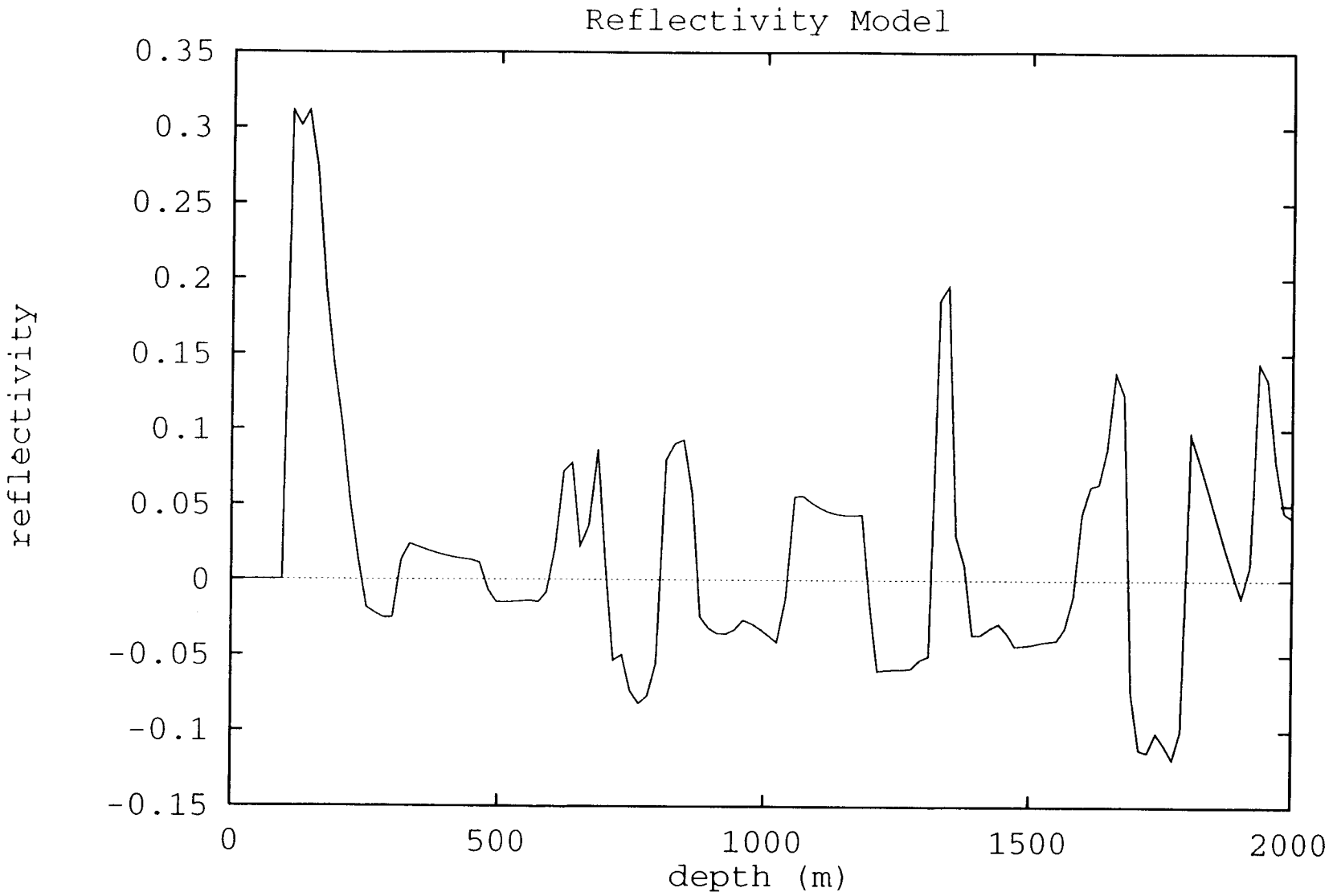
Reflectivity Model
reflectivity
0.35
0.3
0.25
0.2
0.15
0.1
0.05
0
-0.05
-0.1
-0.15
0
500
1000
1500
2000
depth (m)

Figure 5

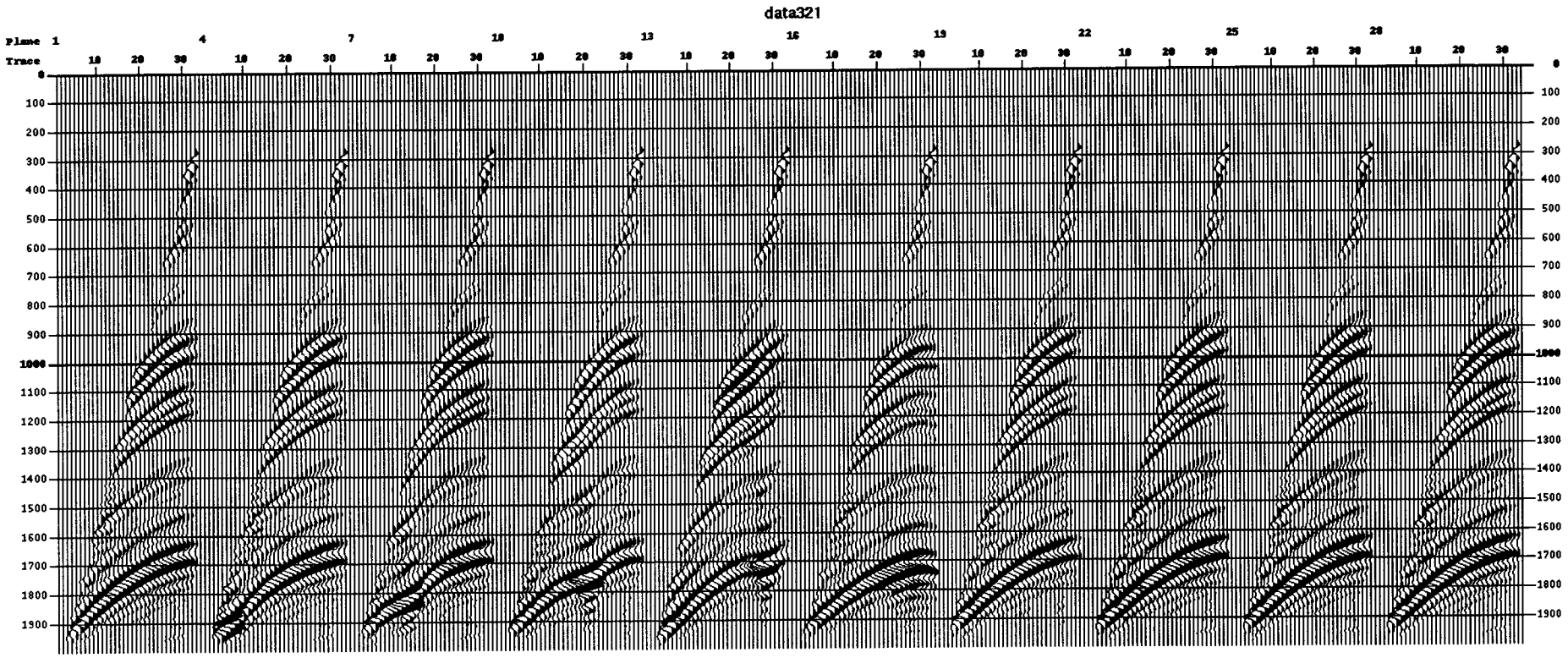
data321
Plane 1 4 7 10 13 16 19 22 25 28
Trace 10 20 30 10 20 30 10 20 30 10 20 30 10 20 30 10 20 30 10 20 30 10 20 30 10 20 30 10 20 30
0 100 200 300 400 500 600 700 800 900 1000 1100 1200 1300 1400 1500 1600 1700 1800 1900

GAS1 – REFLECTIVITY STACK at STRAT

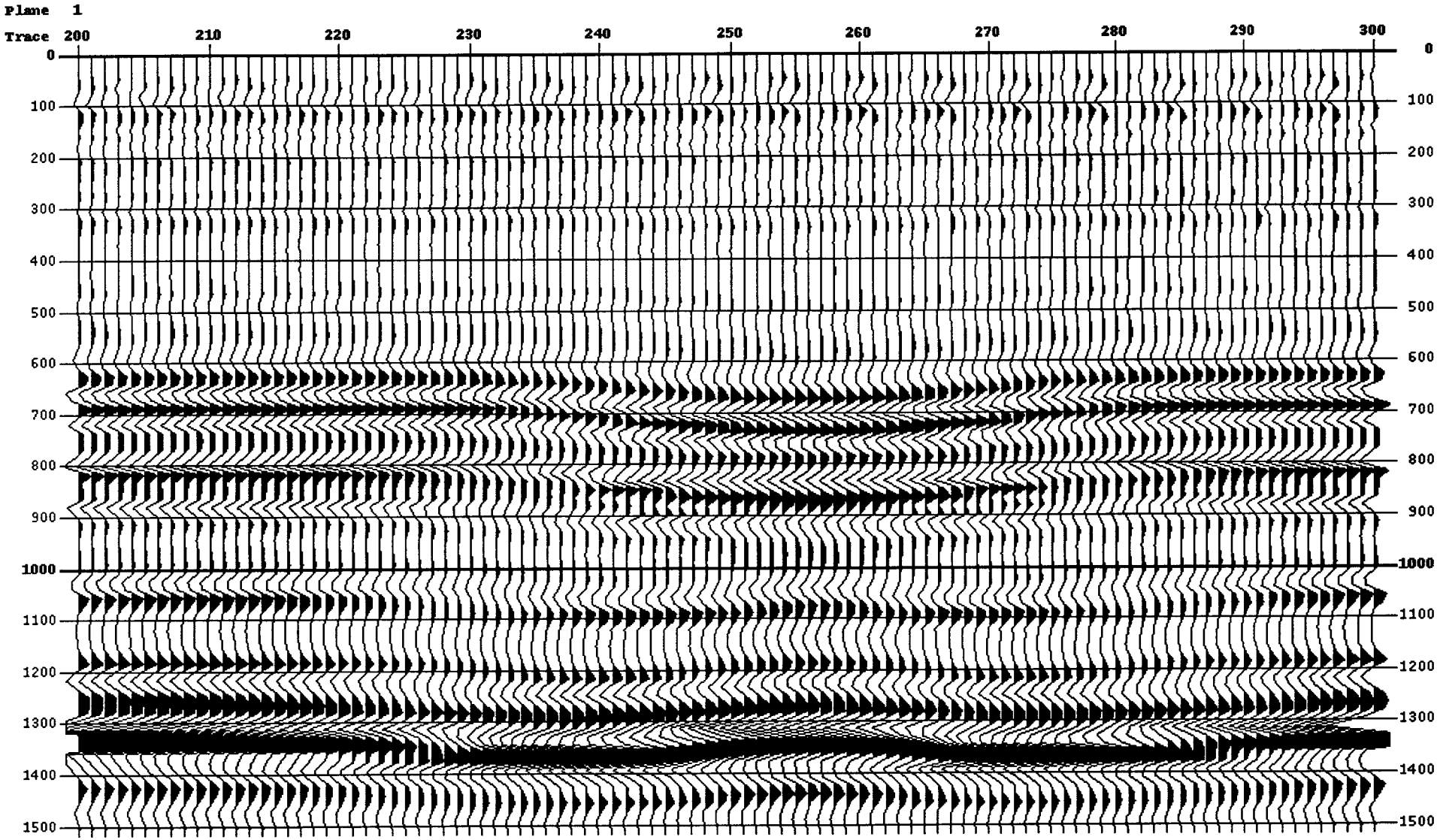

Figure 5

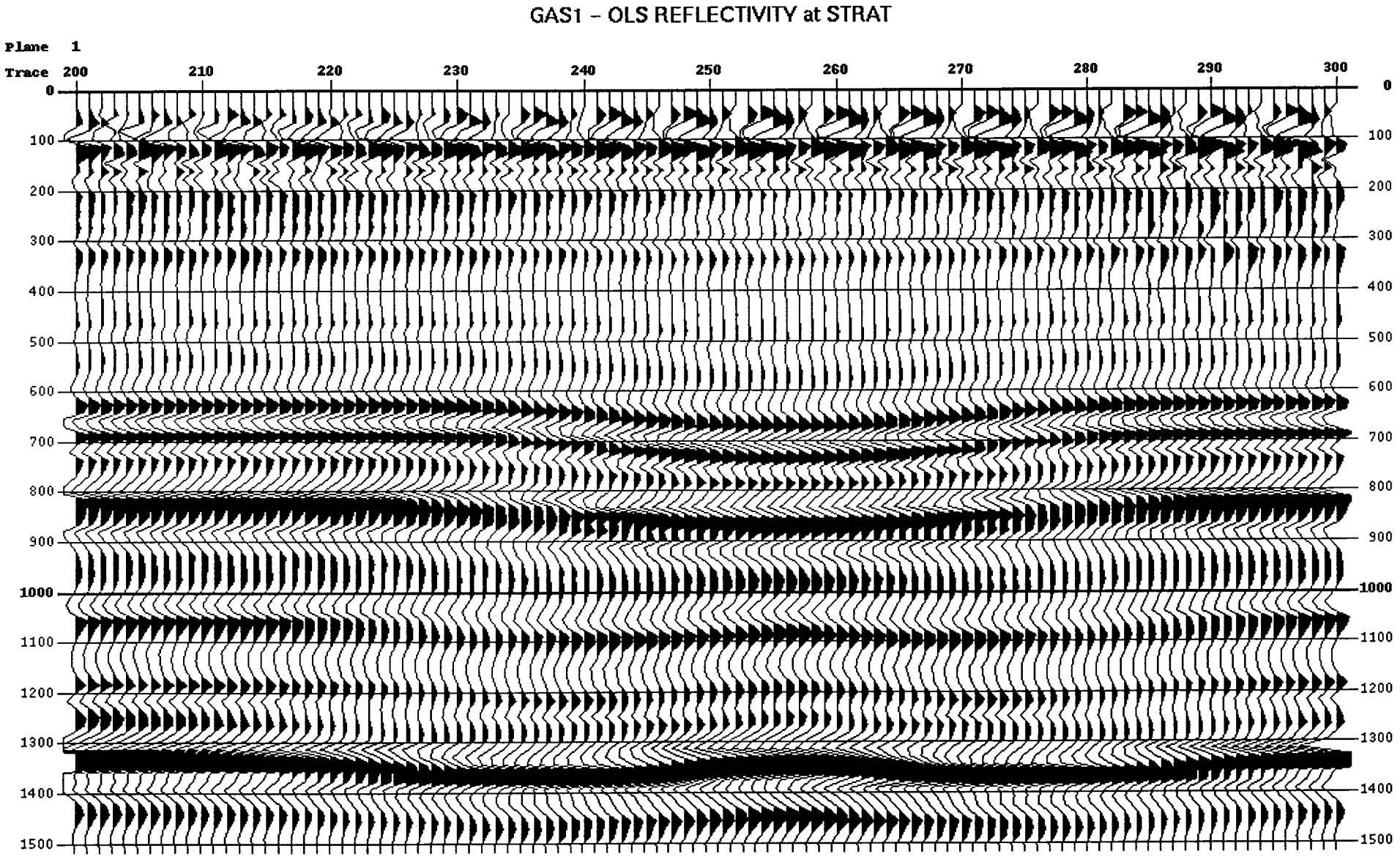
GAS1 – OLS REFLECTIVITY at STRAT
Plane 1
Trace
200
210
220
230
240
250
260
270
280
290
300
0
100
200
300
400
500
600
700
800
900
1000
1100
1200
1300
1400
1500

Figure 6

GAS1 – REFLECTIVITY CDP at STRAT

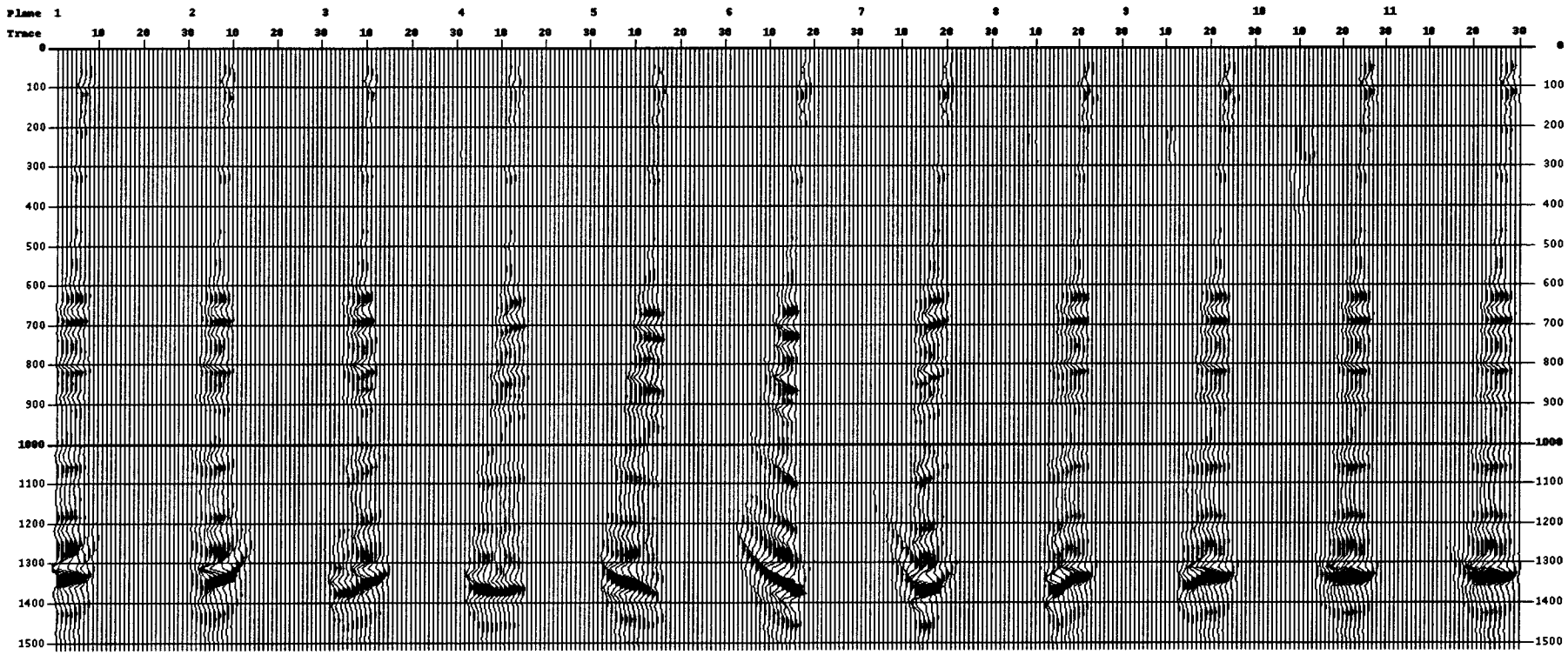

Figure 11

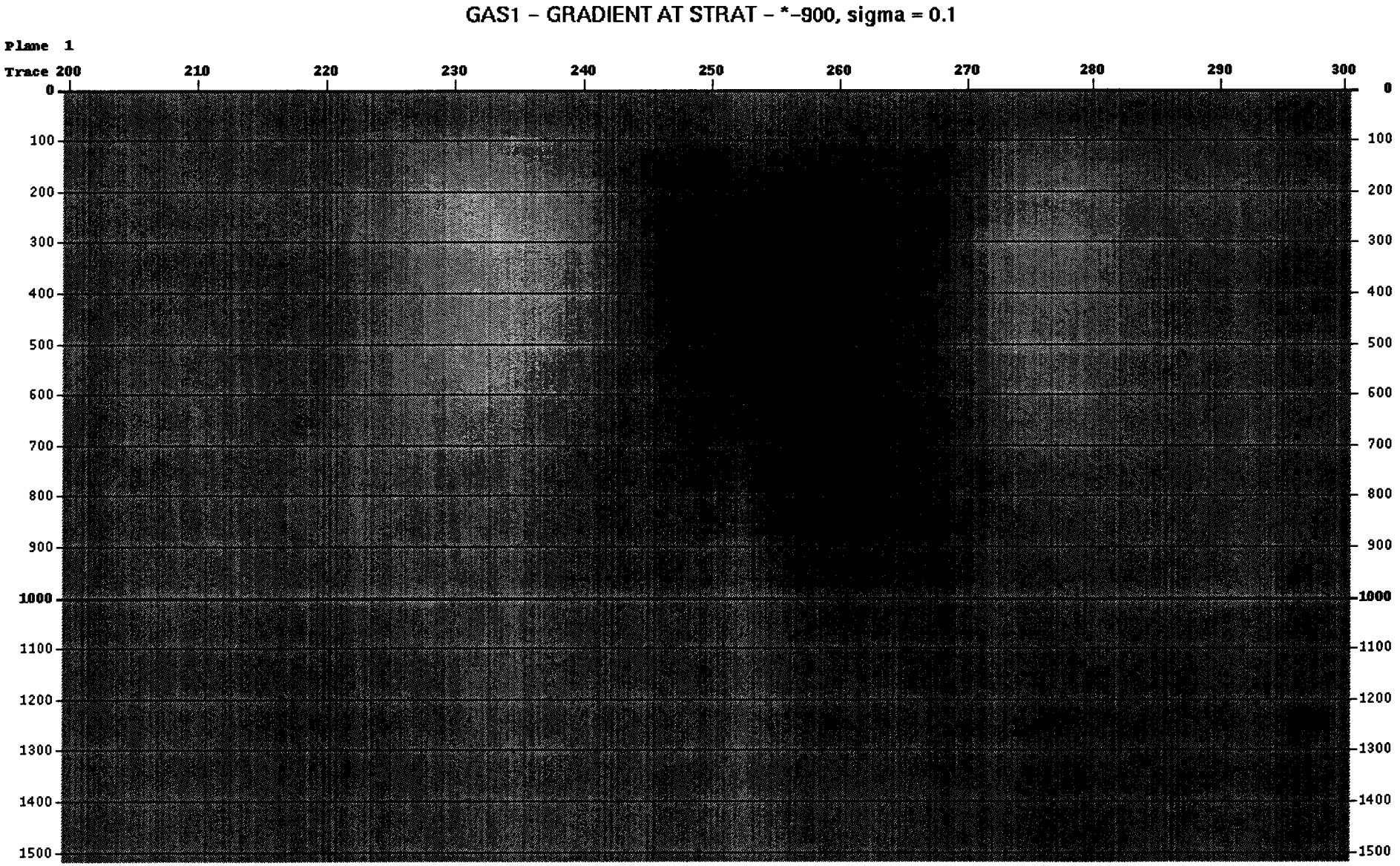
GAS1 – GRADIENT AT STRAT – *–900, sigma = 0.1
Plane 1
Trace 200
210
220
230
240
250
260
270
280
290
300
0
100
200
300
400
500
600
700
800
900
1000
1100
1200
1300
1400
1500

Figure 8

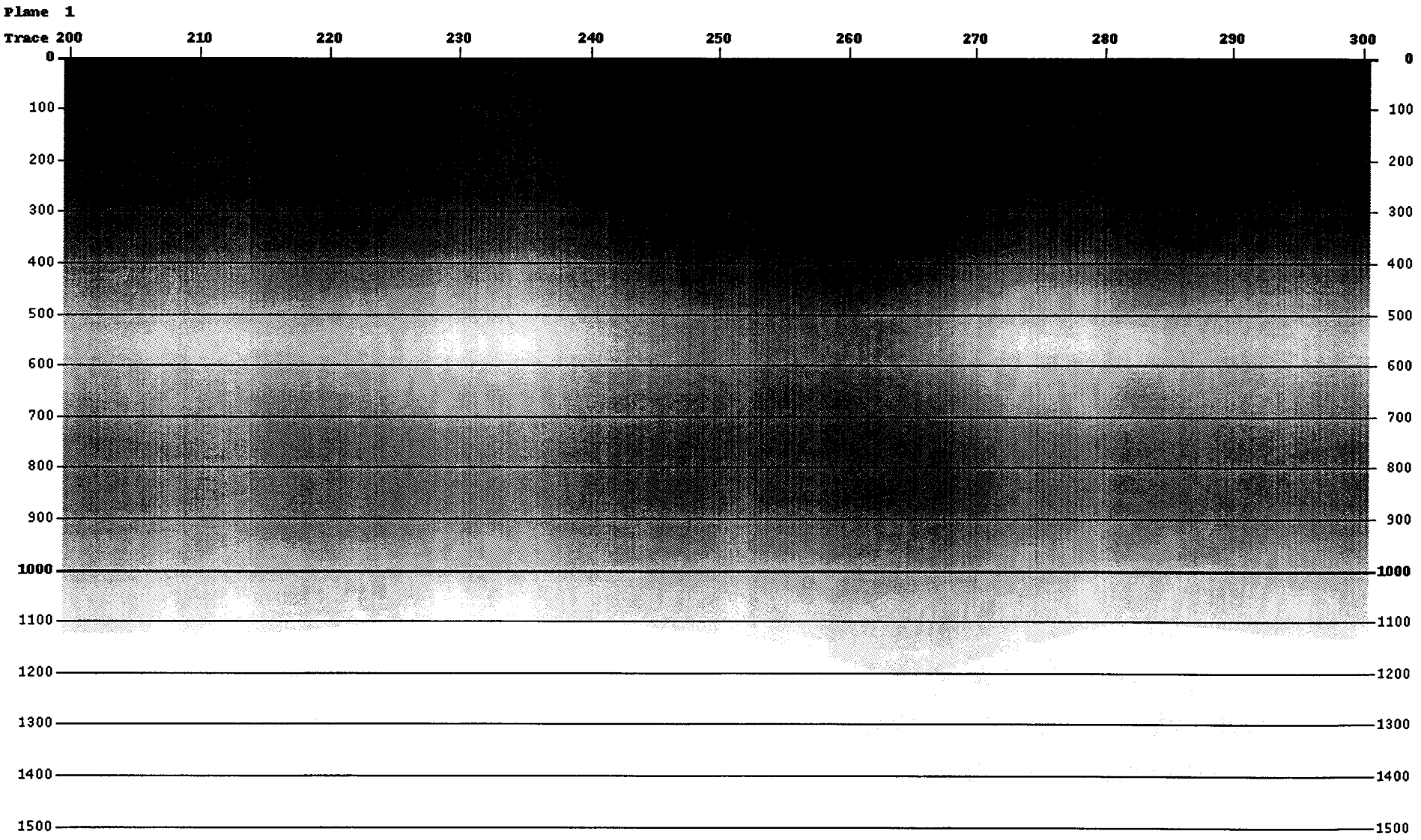
GAS1 – VELOCITY iteration 2
Plane 1
Trace 200
210
220
230
240
250
260
270
280
290
300
0
100
200
300
400
500
600
700
800
900
1000
1100
1200
1300
1400
1500

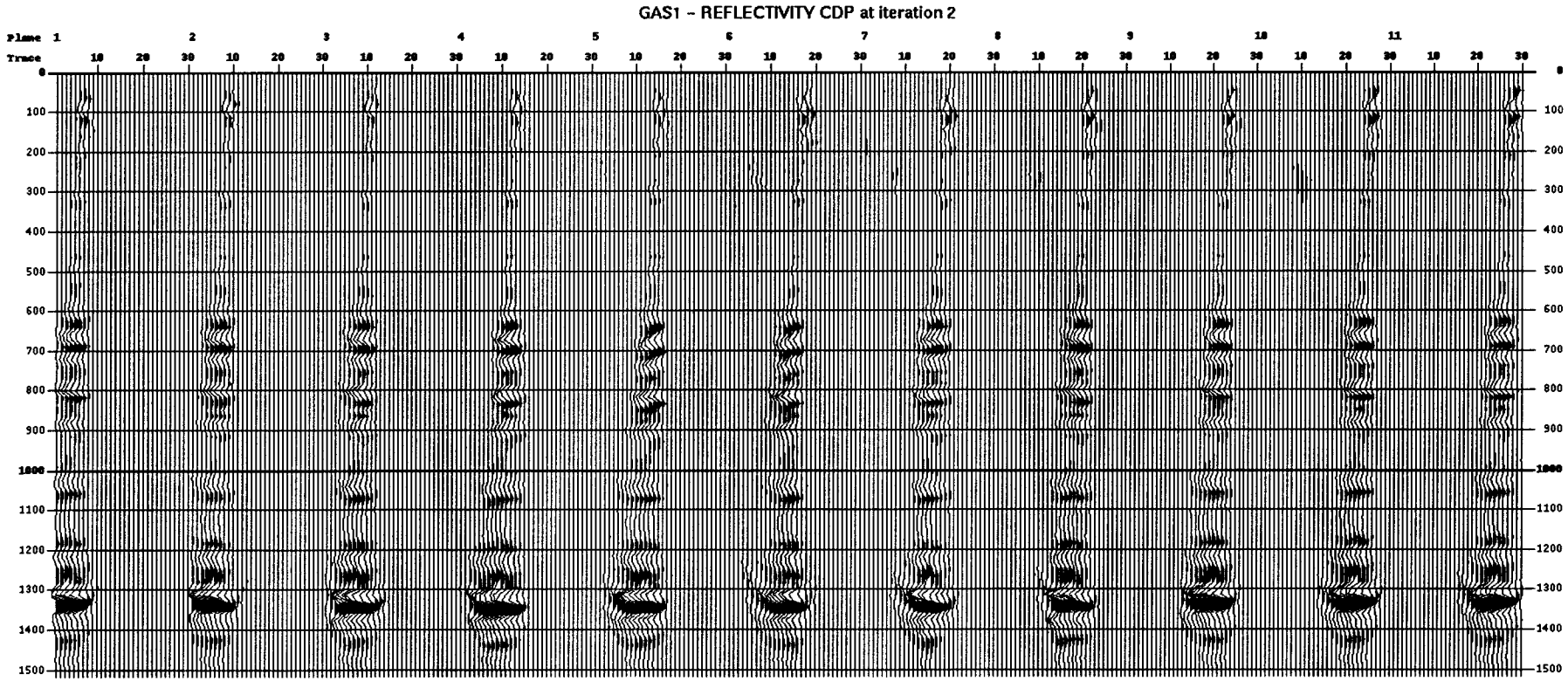
GAS1 - REFLECTIVITY CDP at iteration 2
Plane 1 2 3 4 5 6 7 8 9 10 11
Trace 10 20 30
0 100 200 300 400 500 600 700 800 900 1000 1100 1200 1300 1400 1500

Figure 10

GAS1 – REFLECTIVITY STACK at iteration 2